energies

*Article*

# State of Charge Dual Estimation of a Li-ion Battery Based on Variable Forgetting Factor Recursive Least Square and Multi-Innovation Unscented Kalman Filter Algorithm

**Hongyuan Yuan [1,2,*], Youjun Han [1,3], Yu Zhou [1], Zongke Chen [4], Juan Du [1] and Hailong Pei [1,*]**

1 School of Automation Science and Engineering, South China University of Technology, Guangzhou 510640, China; hanyoujun@gziit.ac.cn (Y.H.); zhouyu2@gedi.com.cn (Y.Z.); dujuan@scut.edu.cn (J.D.)
2 China Energy Construction Group Guangdong Electric Power Design and Research Institute Co., Ltd., Guangzhou 510700, China
3 Guangzhou Institute of Industrial Technology, Guangzhou 511458, China
4 School of Electric Power Engineering, South China University of Technology, Guangzhou 510640, China; tsungkechen@163.com
* Correspondence: hongyuan_yuan@163.com (H.Y.); auhlpei@scut.edu.cn (H.P.)

**Abstract:** Battery management is the key technical link for electric vehicles. A good battery management system can realize the balanced charge and discharge of batteries, reducing the capacity degradation and the loss of health caused by battery overcharge and discharge, which all depend on the real-time and accurate estimation of the battery's state of charge (SOC). However, the battery's SOC has highly complex nonlinear time-varying characteristics related to the complex chemical and physical state and dynamic environmental conditions, which are difficult to measure directly, and this has become a difficulty in design and research. According to the characteristics of ternary lithium-ion batteries of electric vehicles, a battery SOC dual estimation algorithm based on the Variable Forgetting Factor Recursive Least Square (VFFRLS) and Multi-Innovation Unscented Kalman Filter (MIUKF) is proposed in this paper. The VFFRLS algorithm is used to estimate battery model parameters, and the MIUKF algorithm is used to estimate the battery's SOC in real time. The two algorithms are coupled to update battery model parameters and estimate the SOC. The experiment results show that the algorithm has high accuracy and stability.

**Keywords:** equivalent circuit model; multi-innovation; Unscented Kalman Filter; variable forgetting factor recursive least square; SOC online estimation; battery management system



**Citation:** Yuan, H.; Han, Y.; Zhou, Y.; Chen, Z.; Du, J.; Pei, H. State of Charge Dual Estimation of a Li-ion Battery Based on Variable Forgetting Factor Recursive Least Square and Multi-Innovation Unscented Kalman Filter Algorithm. *Energies* **2022**, *15*, 1529. https://doi.org/10.3390/en15041529

Academic Editor: Carlos Miguel Costa

Received: 4 January 2022
Accepted: 17 February 2022
Published: 18 February 2022



## 1. Introduction

With the reduction in fossil energy reserves and the intensification of environmental pollution, in order to achieve the goal of "carbon neutralization" and optimize the industrial structure and energy structure, countries all over the world have increased their investment in the new energy industry. Among these new technologies, research on electric vehicles is one of the main directions of study. In many aspects of electric vehicles' battery technology, battery management technology is extremely important. A good battery management system can prevent the battery from overcharging and discharging and realize balanced management. Accurate battery SOC estimation is the basis of battery management system design, but a battery's SOC comprises highly complex nonlinear time-varying characteristics, which are difficult to measure directly. Therefore, it has become the focus of design and research.

At present, SOC estimation methods mainly include the ampere hour integration method, the open circuit voltage method, and machine learning-based algorithms such as the neural network algorithm [1], Kalman filter (KF) and its extension based on parameter estimation model and system identification.

The estimation accuracy of the ampere hour integration method mainly depends on the initial SOC value and sensor error accumulation—the initial SOC value is difficult to determine, and the errors will accumulate when the online estimation time is long, resulting in low accuracy. The open circuit voltage method uses the functional mapping relationship between the battery open circuit voltage (OCV) and the SOC to estimate the SOC. The error of this method is large when it is used for real-time estimation, because the determined functional relationship requires the battery to be at rest for a long time. The algorithm based on machine learning needs a large number of labeled sample data. Benchmark SOC, which is necessary for use as labeling data, is difficult to obtain through online metrics [2,3], while the cost of obtaining a large number of labeled data in the experimental environment is high, meaning that the research and applications are limited at present. KF uses the recursive method of "prediction-actual measurement-correction", which is more suitable for the dynamic system state estimation such as battery SOC estimation. By establishing the battery models and estimating the parameters, the prior state probability determined by the system model parameters is updated according to the measured a posteriori state probability. Therefore, it has been widely used and has become the mainstream research direction in the field of SOC estimation in recent years.

The KF algorithm assumes that the system is a linear system, but the SOC estimation of the battery is the state estimation of a typical nonlinear time-varying system, so the KF algorithm will introduce linear errors. To solve this problem, many improved methods have been proposed, mainly extending and expanding within the framework of the KF algorithm. Among them, the extended Kalman filter (EKF) and Unscented Kalman Filter (UKF) are widely used. The EKF linearizes the nonlinear system through Taylor series expansion. After ignoring the second-order and higher-order terms, it is transformed into the KF algorithm. The EKF algorithm involves the heavy calculation workload of the Jacobian matrix and ignores the high-order terms. It is suitable for systems with weak nonlinearity because it is easy to cause filter divergence to systems with strong nonlinear systems in addition to introducing linear errors [4–6]. For a strong nonlinear system, based on the idea that the probability density function distribution of the approximate nonlinear function is easier to obtain than the approximate nonlinear function, the UKF algorithm is proposed. This algorithm analyzes the probability density of the functional relationship in the battery model and obtains the set of sampling points around the estimated value through unscented transformation. The statistical characteristics of the variables to be estimated are approximated by a series of sampling points, which avoids the complex operation of Jacobian matrix and considers the influence of higher-order terms on the matrix [7–9]. Related research shows that the accuracy of the UKF reaches the second-order Taylor series at least and is higher than the approximate linearization of EKF.

At the same time, the KF algorithm framework assumes that the system is a Markov process, and the process has no memory—that is, the state at the current time is only affected by the state at the previous time—and has nothing to do with the state before the previous time—that is, the system is a complete information system at any time—but the battery's nonlinear time-varying characteristics, dynamic environments and working conditions determine that the SOC estimation cannot strictly meet this assumption. In order to further improve the performance of the estimation algorithm and break through the boundary assumptions of the KF framework, the multi-innovation (MI) identification theory is proposed. When the algorithm updates the parameters, the errors of multiple historical moments are introduced, and the performance is further improved [10].

The KF algorithm framework and its extension are based on the battery model to estimate the a priori probability of SOC. The a priori probability determined by the system model parameters is then updated by the measured a posteriori probability. The variation of the battery model's parameters is one of the main characteristics of the nonlinear time-varying characteristics of battery SOC estimation. Therefore, the accurate and real-time identification of model parameters is the key to the success of the algorithm. Most of the early research used the offline parameter identification method. Offline parameter identification refers to identifying the parameters of the battery model in advance in the laboratory. During the operation of the battery, the corresponding model parameters are transferred for SOC estimation according to the dynamic working state or working environment [11,12]. Offline parameter identification struggles to cover all of the dynamic characteristics in different environments and working conditions, such as the changes in temperature, the health condition of the battery and other factors. In order to solve this problem, an online parameter identification method is proposed. This method identifies the parameters of the battery model in real time and synchronously with the SOC online estimation through the online parameter identification algorithm according to the characteristic parameters such as current, voltage and temperature collected by the sensor during the working process of the battery system. Online parameter identification needs to adapt to the changing environment and operating state and has high requirements for real-time performance [13,14]. Generally, the amount of data used is smaller than offline parameter identification, which may result in lower accuracy. However, due to its ability to better adapt to the characteristics of a nonlinear time-varying battery, it has become the mainstream research direction in recent years. Among various online identification algorithms for battery model parameters, recursive least square (RLS) and its extended algorithm have become the mainstream online identification algorithms due to their advantages of small storage space, a small amount of computation and being suitable for real-time control [15]. There is an important forgetting factor parameter in the RLS algorithm, which is used to determine the influence weight of the previous time on the identification result of the current time. The selection of this parameter has a great impact on the convergence speed and accuracy of the battery's parameters. In the early stage, the trial-and-error method was mainly used to obtain a fixed value. Later, the Variable Forgetting Factor RLS (VFFRLS) algorithm was proposed, which associated the forgetting factor with the algorithm estimation error in the current time window and realized the design of the dynamic forgetting factor [16].

At present, extensive and in-depth research on the SOC estimation algorithm and the battery model parameter identification algorithm has been conducted based on KF framework and its extension, but most of the research is focused on one aspect, and there is less research on dual or joint estimation algorithms integrating SOC estimation and parameter identification. Recently, a multi-scale EKF joint estimation SOC algorithm [17] and a UKF and VFFRLS joint estimation algorithm [18] were proposed, but there is no dual or joint estimation method that further integrates MI, UKF and VFFRLS. This paper attempts to integrate advantageous algorithms of MI, UKF and VFFRLS and creatively realize the dual estimation experiment of MIUKF + VFFRLS. The experiment results show that the algorithm has obvious advantages in accuracy and stability compared with offline parameter + EKF, offline parameter + UKF and offline parameter + MIUKF. Compared with UKF + VFFRLS, it has advantages in convergence speed, accuracy and stability. The overall performance of the fused algorithm is outstanding.

## 2. Battery Model Establishment and Parameter Identification

### *2.1. Battery Model Establishment*

There are two kinds of battery models: the electrochemical model and equivalent circuit model. The electrochemical model abstracts the complex physical and chemical reaction process inside the battery to describe the dynamic characteristics of the battery. Due to the fundamental process experiment, the accuracy of the model is high, but the model is complex, and the amount of calculation is large, which is difficult to meet the requirements of real-time tasks. The equivalent circuit model uses circuit elements such as resistance, capacitance and power supply to form a circuit network to describe the dynamic characteristics of the battery. It can clearly reflect the electrical characteristics of the battery, and the model is relatively simple, meaning that it is suitable and widely used for tasks requiring real-time calculation such as SOC.

A common equivalent circuit model is the n*RC circuit model. The dynamic characteristics of the battery are simulated by N groups of circuits connected in parallel and then connected in series. It can be divided into zero-order, first-order, second-order and multi-order models according to the number of resistance and capacitor groups. The zero-order equivalent circuit network model is also called the Rint model, which is only composed of a voltage source and a resistor in series. The Rint model can only represent the static process of the battery and cannot describe the dynamic characteristics of the battery. The first-order equivalent circuit network model is also called the Thevenin model [19]. This model consists of a group of capacitors and resistors in a parallel circuit, a voltage source and a resistor which are connected in series. The resistance in series simulates ohmic internal resistance, and the combination of capacitors and resistors in parallel simulates polarization internal resistance. The second-order equivalent circuit network, also known as the DP model [20], is composed of two sets of capacitor resistance parallel circuits, one voltage source and one resistance which are connected in series. The series resistance simulates ohmic internal resistance. The two sets of capacitor resistance parallel circuits are used to describe the short-term electrochemical polarization effect and long-term concentration polarization effect of the battery, respectively, which can describe the dynamic characteristics more accurately.

With the increase in model order, the accuracy of the model will increase, but the complexity of the model will also increase. Considering the balance of accuracy and calculation, the DP model is adopted in this paper, and its circuit structure is shown in Figure 1.

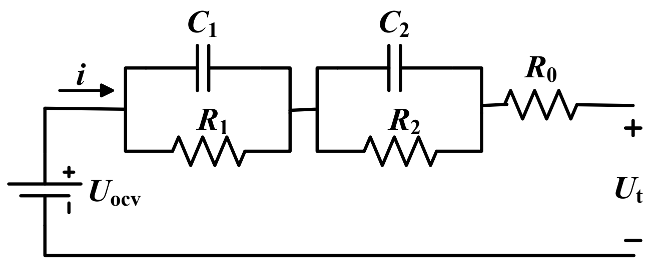


**Figure 1.** DP equivalent circuit model.

It can be seen from the figure that the DP model is composed of a voltage source, ohmic internal resistance and RC networks. $U_{ocv}$ is the battery open circuit voltage. $R_0$ is the battery ohmic internal resistance. $U_t$ is the battery terminal voltage. The parallel network constructed by $R_1$ and $C_1$ is used to reflect the gradual change in the battery terminal voltage, and its time constant is relatively large, which is used to describe the long-term concentration polarization effect. The parallel network constructed by $R_2$ and $C_2$ is used to reflect the sudden change in the battery terminal voltage, and its time constant is small, which is used to describe the short-term electrochemical polarization effect.

According to Kirchhoff's law, the output voltage relation of the DP model is as follows:

$$\begin{cases} U_t = U_{ocv} - IR_0 - U_1 - U_2 \\ \dot{U}_1 = -\frac{1}{C_1 R_1} U_1 + \frac{1}{C_1} I \\ \dot{U}_2 = -\frac{1}{C_2 R_2} U_2 + \frac{1}{C_2} I \end{cases} \quad (1)$$

where $\dot{U}_1$ and $\dot{U}_2$ are the derivatives of $U_1$ and $U_2$ with respect to time, respectively.

*2.2. Open Circuit Voltage Parameter Identification of Battery Model*

The open circuit voltage $U_{ocv}$ is an ideal power supply in the battery model. It is not affected by the resistance capacitance parameters of the battery. It can be measured by the terminal voltage when the battery discharge current is close to zero, and the internal chemical reaction is stable because when the chemical reaction is stable, the dynamic characteristics of the reaction are close to zero. According to Formula (1), $U_{ocv}$ is equal to $U_t$.

There is a relatively stable functional relationship between the open circuit voltage $U_{ocv}$ and SOC. The functional relationship between SOC and $U_{ocv}$ can be obtained by function fitting (generally polynomial fitting) of SOC and $U_{ocv}$ measured at different SOC value points after sufficiently long relaxation.

This functional relationship can be used in battery resistance capacitance parameter identification and SOC estimation.

### *2.3. Resistance Capacitance Parameter Identification of Battery Mode*

Offline parameter identification and online parameter identification can be adopted in the resistance capacitance parameter identification of the battery model. The principles are to use the resistance capacitance parameters of the battery to fit the terminal voltage curve measured in the dynamic charge and discharge process and to optimize the error between the fitting curve and the measured curve through the adjustment of the resistance capacitance parameters. Offline parameter identification is limited by the experimental conditions and cannot cover all situations such as different temperatures, different charge and discharge currents, etc. A large amount of data can be collected for fitting because the real-time performance is not required in the experimental environment, which generally brings high accuracy under the corresponding experimental conditions but may bring sharply dropping accuracy under different conditions. On the contrary, online parameter identification can be dynamically identified according to the real-time operating conditions, but the real-time requirements limit the data amount for fitting, which generally causes lower accuracy, meaning that proper algorithm design is critical. The online parameter identification method is generally modified and innovated based on the RLS method.

#### 2.3.1. Recursive Least Squares Parameter Identification

The RLS algorithm is developed from the least square (LS) algorithm, and the basic principle is as follows [15].

For discrete linear systems

$$y_{k+1} = \theta_k \Phi_{k+1}^{\theta} + e_{k+1}^{\theta} \tag{2}$$

where $y_{k+1}$ is the output vector of the system, and $\theta_k$ is the model parameter vector to be identified; $\Phi_{k+1}^{\theta}$ is the input data matrix of the system, and $e_{k+1}^{\theta}$ is the error vector.

The optimal value estimated by minimizing the sum of squares of $e_k^{\theta}$ errors is the LS algorithm. The resource consumption of the algorithm will continue to rise until the resources are exhausted if all data sequences are used for the estimation of the length of $\Phi_{k+1}^{\theta}$. RLS is proposed to solve this problem, in which the identification results of the current time and the system input of the next time are used to recursively obtain the system parameter value of the next time. The specific methods are as follows:

$$\begin{cases} K_{k+1}^{\theta} = \frac{P_k^{\theta} \Phi_{k+1}^{\theta}}{\lambda + \left(\Phi_{k+1}^{\theta}\right)^T P_k^{\theta} \Phi_{k+1}^{\theta}} \\ \theta_{k+1} = \theta_k + K_{k+1}^{\theta} e_{k+1}^{\theta} \\ P_{k+1}^{\theta} = \lambda^{-1} P_k^{\theta} - \lambda^{-1} K_{k+1}^{\theta} \left(\Phi_{k+1}^{\theta}\right)^T P_k^{\theta} \end{cases} \tag{3}$$

where $K$ is the algorithm gain, and $P$ is the error covariance matrix of the identification parameters. The $\lambda$ is the forgetting factor, which represents the forgetting degree to the previous identification result and determines the confidence comparison between the old and new sampling data. Its value range is between 0 and 1. When the forgetting factor is 1, it means that the algorithm has no forgetting function, and all data points are used in parameter identification; then, the RLS algorithm degenerates to the LS algorithm. When the forgetting factor is 0, it means that the algorithm will forget all the previous identification results and only use the data of the current time for parameter identification. The selection of forgetting factor has a great impact on the accuracy of parameter identification results.

In the RLS method, the parameter needs to be preset as a fixed value, which has a poor effect in the battery parameter identification with complex working conditions.

#### 2.3.2. Parameter Identification of Variable Forgetting Factor Recursive Least Square Method

The VFFRLS method is an improved algorithm based on the recursive least square method (RLS) used to find the optimal value of the forgetting factor adaptively according to the estimation error in the process of parameter identification [16].

The calculation formula of the variable forgetting factor is as follows.

$$\begin{cases} e_{k+1} = y_{k+1} - \hat{y}_{k+1} \\ L(k+1) = -\rho \frac{\sum\limits_{i=k-S+2}^{k+1} e_i e_i^T}{S} \\ \lambda = \lambda_{\min} + (\lambda_{\max} - \lambda_{\min}) 2^{L(k+1)} \end{cases} \quad (4)$$

where $e_{k+1}$ is the estimation error at $k + 1$ time, $\lambda$ is the forgetting factor, and $\lambda_{\min}$ and $\lambda_{\max}$ are the minimum and maximum forgetting factors, respectively. The larger the $\lambda$ is, the smaller the influence of the system fluctuation on the estimation accuracy of the algorithm; the smaller the $\lambda$ is, the stronger the tracking ability and convergence ability of the algorithm. $\rho$ is the sensitivity factor, and $S$ is the window size. In this paper, we set the value of $\lambda_{\min}$ as 0.9, the value of $\lambda_{\max}$ as 0.995 [18], the value of $\rho$ as 200, and the value of $S$ as 22.

## 3. Battery State of Charge Estimation based on Multi-Innovation and Kalman Filter Framework Algorithm

### *3.1. Definition and Characteristics of a Battery's State of Charge*

SOC refers to the ratio of the remaining charge margin in the battery to the rated charge capacity of the battery. The calculation formula is as follows.

$$SOC = SOC_0 - \frac{1}{Q_N} \int_{\tau=t_0}^{\tau=t} \mu I d\tau \quad (5)$$

where $SOC_0$ is the initial SOC value, $Q_N$ is the maximum discharge capacity, $\mu$ represents coulomb efficiency and generally is set to 1, and $I$ is the load current, and its discharge is specified as positive.

*SOC* can only be estimated through indirect methods with, e.g., voltage and current as inputs, which is related to resistance capacitance parameters and working conditions, and so the estimation is related to the ohmic internal resistance, polarization internal resistance, the temperature and health state of the battery, etc. The system has highly complex nonlinear characteristics, and so the estimation error is large if only using the measurement method. If the data of the two dimensions—system state estimation and measurement results—can be used at the same time, the state of the system model over time can be used as an a priori estimation value, the measured value is updated as an a posteriori estimate, and the algorithm should have a very efficient performance improvement in theory. A Bayesian filter has such characteristics. A Bayesian filter can be derived from the Bayesian full probability formula without any omission of the nonlinear characteristics of the system, but it is difficult to obtain the prior probability distribution of the system in practical use, and the calculation is also too complex. In order to facilitate calculation, in practical application, it is generally assumed that the probability distribution is normally distributed, and the system is a complete information system—that is, the state of the next time is only related to the current time. In this case, the algorithm is simplified to the KF algorithm.

KF and its extended algorithm adopt the recursive filtering algorithm, which has the characteristics of simple calculation. At the same time, the algorithm uses the data of two relatively independent dimensions—state equation and measurement equation—for verification and updating, which can effectively improve the accuracy of the algorithm. Therefore, it is widely used in SOC estimation.

### 3.2. Kalman Filter

The basic formula of KF is as follows:

$$x_{k+1} = A_{k+1}x_k + B_{k+1}u_{k+1} + \omega_{k+1} \tag{6}$$

$$y_{k+1} = H_{k+1}x_{k+1} + v_{k+1} \tag{7}$$

where Equation (6) is called the state equation, and Equation (7) is called the measurement equation. $x_k$ is the state vector at time $k$, $x_{k+1}$ is the state vector at time $k$ + 1, $y_{k+1}$ is the observation vector at time $k$ + 1, $u_{k+1}$ is the system input vector at time $k$ + 1, $A$ is the state transition parameter matrix, $B$ is the input control parameter matrix, $H$ is the observation parameter matrix, $\omega_{k+1} \sim N(0, Q_{k+1})$ is the system noise vector, and $v_{k+1} \sim N(0, R_{k+1})$ is the measurement noise vector. $\omega_{k+1}$ and $v_{k+1}$ are independent of each other.

The recursive process of the algorithm is as follows.

(1) Predict the system state at the next time.

$$\hat{x}_{k+1}^{(-)} = A_{k+1}\hat{x}_k^{(+)} + B_{k+1}u_{k+1} \tag{8}$$

(2) Predict the system covariance at the next time.

$$P_{k+1}^{(-)} = A_{k+1}P_k^{(+)}A_{k+1}{}^T + Q_{k+1} \tag{9}$$

(3) Calculate the Kalman gain of the measurement update.

$$K_{k+1} = \frac{P_{k+1}^{(-)}H_{k+1}{}^T}{H_{k+1}P_{k+1}^{(-)}H_{k+1}{}^T + R_{k+1}} \tag{10}$$

(4) Update the system status by the measured values.

$$\hat{x}_{k+1}^{(+)} = \hat{x}_{k+1}^{(-)} + K_{k+1}(y_{k+1} - H_{k+1}\hat{x}_{k+1}^{(-)}) \tag{11}$$

(5) Update system covariance by the measured values.

$$P_{k+1}^{(+)} = (I - K_{\mathrm{k}+1}H_{k+1})P_{k+1}^{(+)} \tag{12}$$

where $\hat{x}_{k+1}^{(-)}$ represents an a priori estimate of x at time $k$ + 1, $\hat{x}_{k+1}^{(+)}$ represents an a posteriori estimate of $x$ at time $k$ + 1, $\hat{x}_k^{(+)}$ represents an a posteriori estimate of $x$ at time $k$, $P_{k+1}^{(-)}$ represents an a priori estimate of $P$ at time $k$ + 1, $P_{k+1}^{(+)}$ represents an a posteriori estimate of $P$ at time $k$ + 1, and $P_k^{(+)}$ represents an a posteriori estimate of $P$ at time $k$. $K_{k+1}$ represents the Kalman gain at time $k$ + 1.

KF requires that the state equation and measurement equation of the system are linear, which is difficult to apply to nonlinear tasks such as the battery state of charge. Instead, the EKF and UKF algorithms are generally used in such tasks.

### 3.3. Extended Kalman Filter Algorithm

The EKF algorithm is transformed into the KF algorithm by expanding the Taylor series of state and measurement functions and ignoring the second-order and higher-order terms. The basic formula is as follows:

$$x_{k+1} = f(x_k, u_k, k, \omega_k) \tag{13}$$

$$y_{k+1} = h(x_{k+1}, k) + v_{k+1} \tag{14}$$

where $u_k$ is the system input vector at time $k$, $\omega_k \sim N(0, Q_k)$ is the system noise vector, and $v_k \sim N(0, R_k)$ is the measurement noise vector. $\omega_k$ and $v_k$ are independent of each other.

The recursive process of the algorithm is as follows.

(1) Predict the system state at the next time.

$$\hat{x}_{k+1}^{(-)} = f(\hat{x}_k, u_k, k) \tag{15}$$

(2) Predict the system covariance at the next time.

Let

$$F_k = \left.\frac{\partial f}{\partial x}\right|_{x_k = \hat{x}_k^{(+)}} \tag{16}$$

Get

$$P_{k+1}^{(-)} = F_k P_k^{(+)} {F_k}^T + Q_k \tag{17}$$

(3) Calculate the Kalman gain of the measurement update.

Let

$$H_{k+1} = \left.\frac{\partial h}{\partial x}\right|_{x_{k+1} = \hat{x}_{k+1}^{(-)}} \tag{18}$$

Get

$$K_{k+1} = \frac{P_{k+1}^{(-)} {H_{k+1}}^T}{H_{k+1} P_{k+1}^{(-)} {H_{k+1}}^T + R_{k+1}} \tag{19}$$

(4) Update the system status by the measured values.

$$\hat{x}_{k+1}^{(+)} = \hat{x}_{k+1}^{(-)} + K_{k+1}\left\{y_{k+1} - h\left[\hat{x}_{k+1}^{(-)}, k+1\right]\right\} \tag{20}$$

(5) Update system covariance by the measured values.

$$P_{k+1}^{(+)} = P_{k+1}^{(-)} - K_{k+1}\left[H_{k+1} P_{k+1}^{(-)} H_{k+1}^T + R_{k+1}\right] \tag{21}$$

where $\hat{x}_{k+1}^{(-)}$ represents an a priori estimate, and $\hat{x}_{k+1}^{(+)}$ represents an a posteriori estimate of $x$ at time $k + 1$; $\hat{x}_k^{(+)}$ represents an a posteriori estimate of $x$ at time $k$; $P_{k+1}^{(-)}$ represents an a priori estimate of $P$ at time $k + 1$; $P_{k+1}^{(+)}$ represents an a posteriori estimate of $P$ at time $k + 1$, and $P_k^{(+)}$ represents an a posteriori estimate of $P$ at time $k$. $K_{k+1}$ represents the Kalman gain at time $k + 1$.

The EKF algorithm omits the influence of second-order and higher-order terms and is only applicable to the case of weak nonlinearity. For the case of heavy nonlinearity, the error is large, and more complex nonlinear filtering algorithms are often required, such as the UKF.

### 3.4. Unscented Kalman Filter Algorithm

The UKF takes the KF as the basic framework—the basic formula is consistent with that of the EKF, and unscented transformation is applied to realize nonlinear application scenarios. The recursive algorithm flow is as follows.

(1) Let the a posteriori state estimation and covariance at time $k$ be $x_k^{(+)}$ and $P_k^{(+)}$, respectively.

(2) Calculate sampling points.

$$\begin{cases} \chi_k^0 = x_k^{(+)} \\ \chi_k^i = x_k^{(+)} + \sqrt{(L+\eta)P_{xx}}, i = 1, 2 \ldots L \\ \chi_k^i = x_k^{(+)} - \sqrt{(L+\eta)P_{xx}}, i = L+1, L+2, \ldots 2L \end{cases} \tag{22}$$

where $L$ is the length of the state vector, and the weight value is calculated as follows:

$$\begin{cases} \eta = \alpha^2(L+k_i) - L \\ W_m^0 = \frac{\eta}{L+\eta}, W_m^i = \frac{1}{2(L+\eta)}, i = 1, 2 \ldots 2L \\ W_c^0 = \frac{\eta}{L+\eta} + 1 - \alpha^2 + \beta, W_c^i = \frac{1}{2(L+\eta)}, i = 1, 2 \ldots 2L \end{cases} \tag{23}$$

where subscript $c$ represents the weight of covariance; subscript $m$ represents the weight of mean square deviation; $\eta$ represents the scaling ratio, and $\alpha$ represents the distribution state of sampling points—when $\alpha$ is large, it indicates a greater weight of sigma points at the average value. $\beta$ is a weight, which is used to combine the dynamic differences of higher-order terms in the equation. In this paper, we set $L$ = 3, $\alpha$ = 0.01, $k_i$ = 0, $\beta$ = 2.

(1) Update the a priori state value $x_{k+1}^{(-)}$ and a priori variance value $P_{k+1}^{(-)}$.

$$\chi_{k+1}^i = f(\chi_k^i, u_k, k) \tag{24}$$

$$x_{k+1}^{(-)} = \sum_{i=0}^{2L} W_m^i \chi_{k+1}^i \tag{25}$$

$$P_{k+1}^{(-)} = \sum_{i=0}^{2L} (W_c^i (\chi_k^i - x_{k+1}^{(-)})(\chi_k^i - x_{k+1}^{(-)})^T) + Q_{k+1} \tag{26}$$

where $Q_k$ is the system noise covariance matrix; in this paper, we set $Q_k$= 0.00000001 $*$ $\begin{bmatrix} 1 & 0 & 0 \\ 0 & 1 & 0 \\ 0 & 0 & 1 \end{bmatrix}$.

(2) Calculate the observation estimation value $\hat{y}_{k+1}$, observation variance prediction value $P_{k+1}^{yy}$ and estimated covariance difference $P_{k+1}^{xy}$.

$$y_{k+1}^i = h(\chi_{k+1}^i, k+1) \tag{27}$$

$$\hat{y}_{k+1} = \sum_{i=0}^{2L} W_m^i y_{k+1}^i \tag{28}$$

$$P_{k+1}^{yy} = \sum_{i=0}^{2L} (W_c^i (y_{k+1}^i - \hat{y}_{k+1})(y_{k+1}^i - \hat{y}_{k+1})^T + R_{k+1} \tag{29}$$

$$P_{k+1}^{xy} = \sum_{i=0}^{2L} W_c^i (\chi_{k+1}^i - \hat{x}_{k+1}^{(-)})(y_{k+1}^i - \hat{y}_{k+1})^T \tag{30}$$

where $R_k$ is the measurement noise covariance matrix; in this paper, we set $R_k = 1$.

(3) Update the a posteriori state value $x_{k+1}^{(+)}$ and a posteriori state error covariance $P_k^{(+)}$ using the measured value $y_{k+1}$.

$$K_{k+1} = \frac{P_{k+1}^{xy}}{P_{k+1}^{yy}} \tag{31}$$

$$x_{k+1}^{(+)} = x_{k+1}^{(-)} + K_{k+1}(y_{k+1} - \hat{y}_{k+1}) \tag{32}$$

$$P_{k+1}^{(+)} = P_{k+1}^{(-)} - K_{k+1} P_{k+1}^{yy} K_{k+1} \tag{33}$$

where $K_{k+1}$ represents Kalman gain at time $k + 1$.

Compared with the EKF algorithm, the UKF can adapt to systems with stronger nonlinearity and can achieve third-order approximation accuracy in the case of Gaussian distribution and second-order approximation accuracy in the case of non-Gaussian distribution; the UKF does not need to calculate the Jacobian matrix, but the number of sampling points is $2n + 1$, and the overall amount of calculation is larger than the EKF algorithm.

### *3.5. Application of Multi-Innovation in Kalman Filter Framework Algorithm*

In the traditional KF framework algorithm, only the error of the current time is used to update the state of the next time. The model is simple and easy to calculate, but it also brings problems. For highly complex nonlinear time-varying battery operating conditions, the state of the next time is likely to be related not only to the current time but also to several times before the current time, resulting in a decline in accuracy. In order to solve the problem and further improve the estimation progress, the multi-innovation identification theory is introduced into the measurement equation. The calculation formula of multi-innovation identification is as follows.

Expand a single innovation $e_k$ into an innovation matrix $e_{p,k}$.

$$e_{p,k} = \begin{bmatrix} e_k \\ e_{k-1} \\ e_{k-2} \\ \vdots \\ e_{k-p+1} \end{bmatrix} \tag{34}$$

At the same time, the gain $k_k$ is extended to the gain matrix $k_{p,k}$

$$k_{p,k} = \left[ k_k, k_{k-1}, \cdots, k_{k-\mathrm{p}+1} \right] \tag{35}$$

Therefore, the status measurement update needs to be modified as follows:

$$y_k = \hat{y}_k + \left[ \mathrm{k}_k, k_{k-1}, \cdots k_{k-\mathrm{p}+1} \right] e_{p,k} \tag{36}$$

Namely,

$$y_k = \hat{y}_k + \sum_{i=0}^{p} \gamma_{\mathrm{i}} k_{i,k} e_{k-i} \tag{37}$$

where

$$\begin{cases} \gamma_1 = 1 \\ \gamma_2 = \gamma_3 = \cdots \gamma_p = \frac{a}{M-1}, 0 \le a \le 1, M \ge 2 \end{cases} \tag{38}$$

where $M$ is the innovation length and $a$ is the adjustable coefficient. This paper takes $M$ as 22and takes $a$ as 0.5. A detailed discussion about the selection of the two parameters will be conducted in Section 5.3.1.

## **4. Dual Estimation of VFFRLS Battery Model Parameters and MIUKF Battery SOC**

### *4.1. Union of Basic Equations*

It can be obtained from Equations (2) and (14) that

$$\theta_k \Phi_{k+1}^{\theta} + e_{p,k+1} = h(x_{k+1}^{(-)}, k+1) + v_{k+1} \tag{39}$$

Then, it can be obtained from Equation (13) that

$$\theta_k \Phi_{k+1}^{\theta} + e_{p,k+1} = h(f(x_k^{(+)}, u_k, \omega_k, k)) + v_{k+1} \tag{40}$$

Finding partial derivatives on both sides of the equation,

$$\Phi^{\theta}_{k+1} + \frac{\partial}{\partial \theta_k} e_{p,k+1} = \frac{\partial}{\partial \theta_k}\left(h(f(x^{(+)}_k, u_k, \omega_k, k)\right) + \frac{\partial}{\partial \theta_k} v_{k+1} \tag{41}$$

where $e_{p,k}$,$\omega_{k-1}$, and $v_k$ are defined as being independent of $\theta_k$. Equation (42) can be simplified to

$$\Phi^{\theta}_{k+1} = \frac{\partial}{\partial \theta_k}\left(h(f(x^{(+)}_k, u_k, k)\right) \tag{42}$$

Thus, the basic equations of VFFRLS battery model parameter estimation and MIUKF SOC estimation are combined.

### 4.2. Setting of Estimation Period

Compared with the time-varying characteristics of SOC, the time-varying characteristics of battery parameters are relatively flat, and the time interval for updating the estimation can be relatively long. In the dual estimation, the SOC estimation is carried out for each sampling period while the estimation of battery parameters adopts multiple sampling intervals as $T_\theta$, which is taken as 60 in this paper.

### 4.3. Battery Parameters Transmission

Every time the battery parameters are updated, the VFFRLS part of the algorithm passes the current battery parameters to the SOC estimation and starts the timer. Before reaching the sampling interval set by the timer, the battery parameters remain unchanged—that is, if the update time parameter is $\theta_k$, the subsequent parameters $\theta_{k+1}$, $\theta_{k+2} \ldots \theta_{k+T_\theta-1}$ are equal to $\theta_k$.

### 4.4. Forgetting factor Transmission

The timer starts after the battery parameter is updated. When the sampling interval set by the timer is reached, the battery parameter will be updated again. At this time, the SOC estimation part of the algorithm transmits the error in the previous M sampling cycle time window to the VFFRLS part of the algorithm to calculate the forgetting factor $\lambda$, which can then be substituted into the parameter in the equation.

### 4.5. Algorithm Flow

The algorithm flow is shown in Figures 2–4.

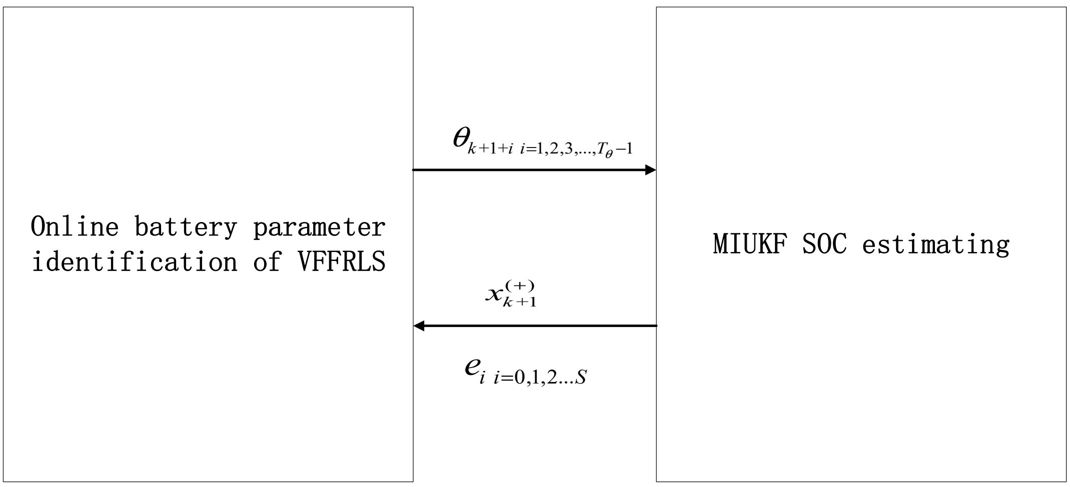


**Figure 2.** Overall block diagram of algorithm.

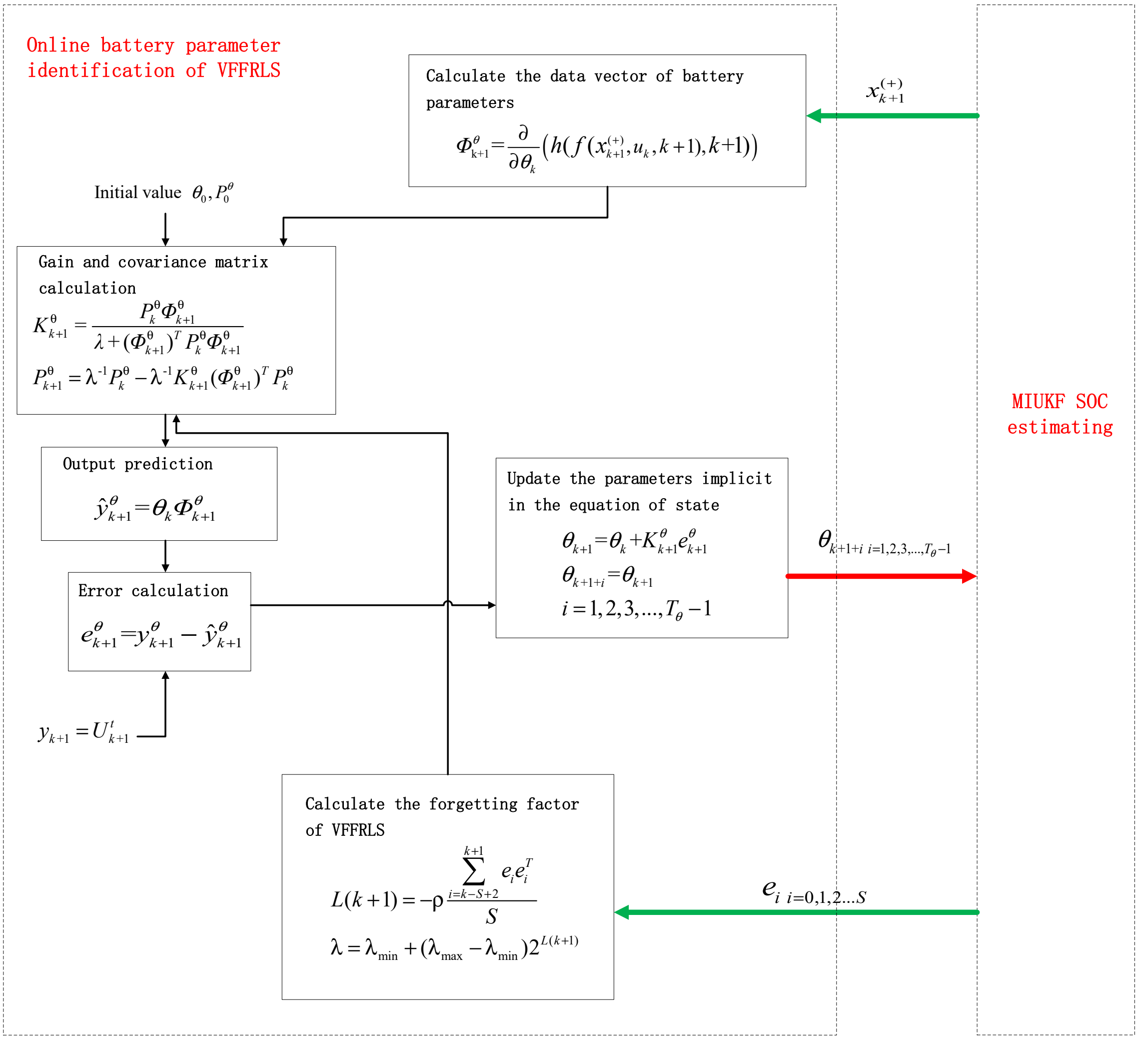


**Figure 3.** The algorithm flow of VFFRLS part.

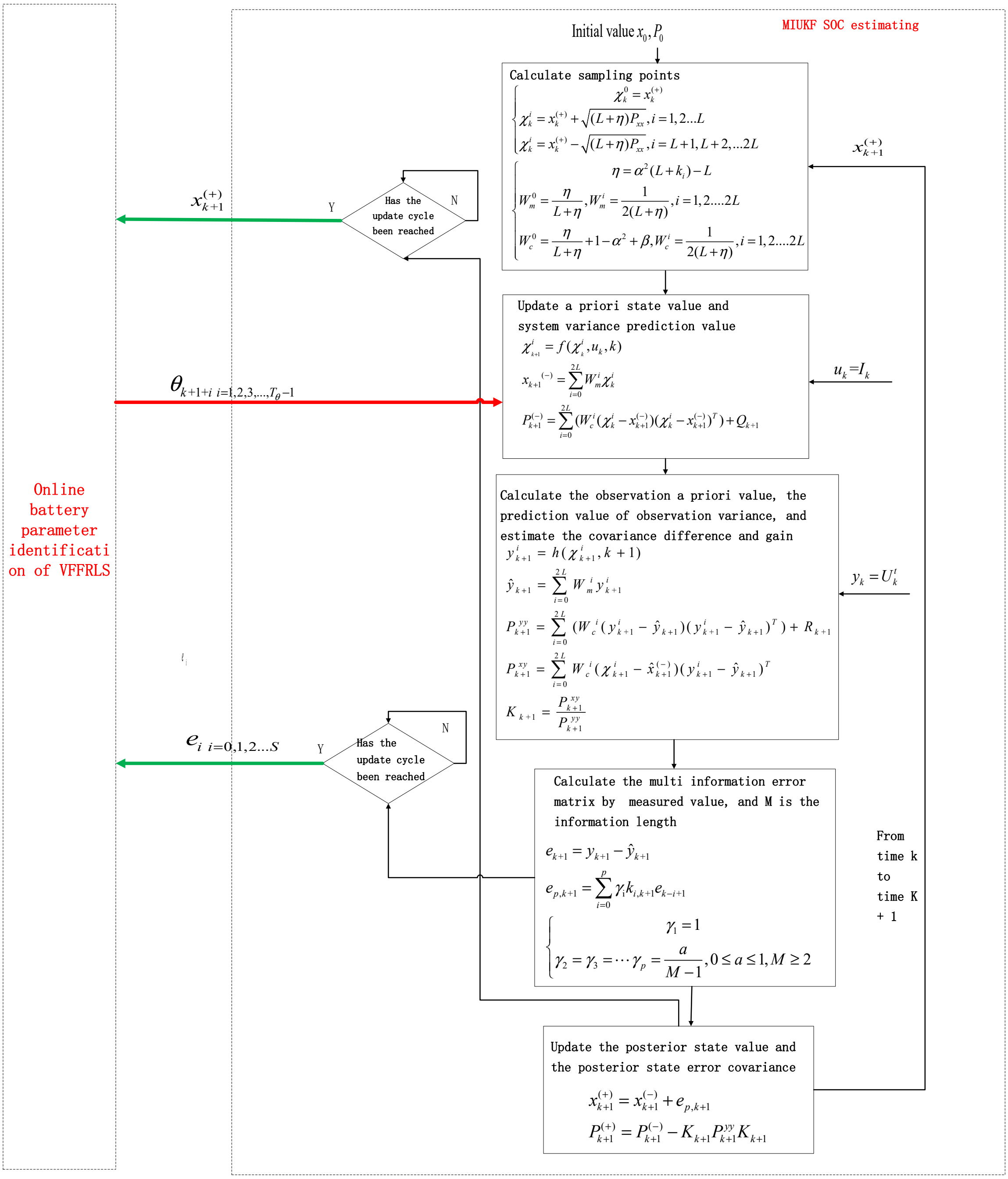


**Figure 4.** The algorithm flow of MIUKF part.

## 5. Analysis of Experiment Results

### 5.1. Data Sources and Tools

The battery used in this paper is a 32 Ah/3.7 V square ternary material lithium power battery produced by Ningde Times. The test platform consists of a battery cell, a power battery test system and a high- and low-temperature damp heat alternating test chamber. In this paper, the effectiveness of the algorithm is verified by using the Urban Dynamometer Driving Schedule (UDDS) [21] cycle test data. The test conditions are set to 25 °C. After the battery is fully charged and left to stand for half an hour, it is discharged for 13 UDDS cycle cycles, the SOC is reduced from 100% to 1.2%, the voltage is reduced from 4.18 V to 3.21 V, the experimental data acquisition interval is set as 1 s, and a total of 20,000 data samples are collected. The algorithm is simulated by MATLAB R2019b based on the collected data.

*5.2. Model Substitution*

Let $\left[U_1^k, U_2^k, SOC^k\right]^T$ be the basic form of the state vector $x_k$ and the observation vector $y_k$ at time $k$, and the battery parameter matrix $\theta_k = [R_0^k, R_1^k, C_1^k, R_2^k, C_2^k]^T$ is embedded into the state equation as an intermediate variable through the functional relationship with $U_1^k$, $U_2^k$, $SOC^k$ and $I_k$. The initial setting value of $x_k = \left[U_1^k, U_2^k, SOC^k\right]^T$ is $[0, 0, 0.8]^T$, and the initial value of $\theta_k$ is obtained from offline identified parameters, that is $[0.002, 0.0012, 7.23e + 04, 0.0011, 4.49e + 04]^T$, while the initial variance of $\theta_k$ is set as $P_0 = [0.0001, 0.0001, 10000, 0.0001, 10000]^T$.

The measured data are a matrix composed of vectors $\left[k, I^k, U_t^k, Soc_r^k\right]^T$. $I_k$ is substituted into the measurement equation as the input vector at time $k$. $U_t^k$ is substituted into the measurement equation through the functional relationship with $U_1^k$, $U_2^k$ and $U_{ocv}^k$, and the functional relationship between $U_{ocv}^k$ and $Soc^k$. The data provided by the original factory for fitting the functional relationship between SOC and OCV are shown in Table 1.

**Table 1.** Relationship data between SOC and OCV.

| Uocv | 3.423 | 3.521 | 3.596 | 3.644 | 3.696 | 3.784 | 3.88 | 3.948 | 4.02 | 4.075 | 4.181 |
|---|---|---|---|---|---|---|---|---|---|---|---|
| SOC | 0 | 0.1 | 0.2 | 0.3 | 0.4 | 0.5 | 0.6 | 0.7 | 0.8 | 0.9 | 1 |

Under the experimental condition, one discharge cycle is tested, so there are no long-term cumulative error problems. Then, $Soc_r^k$, which is obtained from the ampere hour integral method, has high accuracy and can be used as the benchmark for the comparison of the algorithm results.

The data are then substituted into the Kalman filter framework algorithm. The essence of the error is the difference between the a priori state terminal voltage determined by the battery resistance capacitance parameter and the measured terminal voltage, which is characterized by the difference between the a priori state value and the measured value. The task of this paper is to update the resistance capacitance parameters and Kalman filter parameters through the iterative process of the VFFRLS + MIUKF algorithm to minimize the terminal voltage error.

*5.3. Experiment Result*

5.3.1. Experiment Results of Different Parameters of MI

According to Formula (38), the parameters $M$ and a are the key parameters affecting the multi-innovation model, and their value and influence need to be analyzed. In the following, nine parameters are selected for an interval 20 of $M \in$ [2162], and eleven parameters are selected for an interval 0.1 of $a \in$ [0,1] for combined analysis. When $a$ = 0, the multi-innovation model does not work. At this time, MIUKF + VFFRLS degenerates into the UKF + VFFRLS algorithm. Therefore, the comparison of the two algorithms can be transformed into the comparison of algorithms when $a$ is non-zero and a is zero.

The nine values of M are classified, and different values of a are taken in each classification, substituted into the model, and the final SOC error is calculated to draw a three-dimensional diagram (in order to ensure the image display effect, the data at 41 to 20,000 time points are intercepted in $t$ dimension). The results are shown in Figure 5.

At the same time, the average and standard deviation of the absolute value of SOC error under different parameter values are calculated. Among them, the average value of the absolute value of SOC error under different parameter values is shown in Table 2.

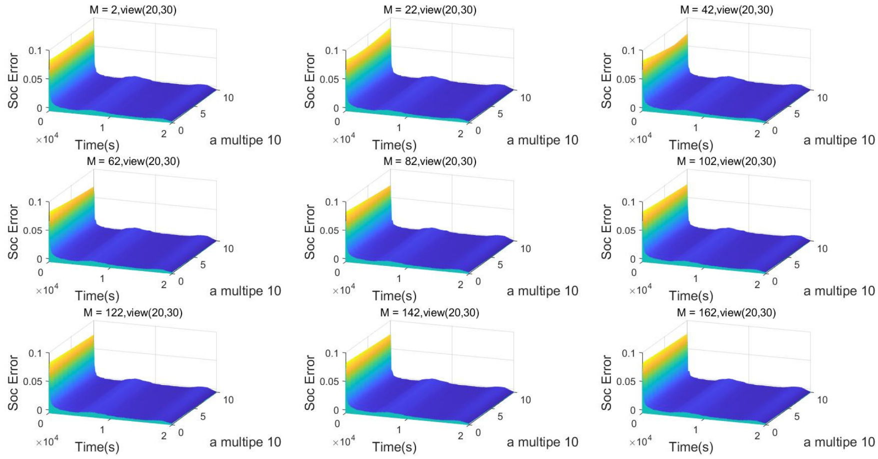


**Figure 5.** Variation of SOC error with time under different value combinations of *M* and *a*.

**Table 2.** Average value of the absolute value of SOC error under different parameter values.

| | $M = 2$ | $M = 22$ | $M = 42$ | $M = 62$ | $M = 82$ | $M = 102$ | $M = 122$ | $M = 142$ | $M = 162$ |
|---|---|---|---|---|---|---|---|---|---|
| $a = 0$ | 0.247% | 0.247% | 0.247% | 0.247% | 0.247% | 0.247% | 0.247% | 0.247% | 0.247% |
| $a = 0.1$ | 0.230% | 0.229% | 0.228% | 0.227% | 0.226% | 0.224% | 0.223% | 0.221% | 0.220% |
| $a = 0.2$ | 0.224% | 0.223% | 0.222% | 0.220% | 0.218% | 0.216% | 0.214% | 0.212% | 0.210% |
| $a = 0.3$ | 0.223% | 0.221% | 0.220% | 0.218% | 0.216% | 0.214% | 0.211% | 0.209% | 0.207% |
| $a = 0.4$ | 0.223% | 0.222% | 0.221% | 0.219% | 0.217% | 0.215% | 0.213% | 0.211% | 0.209% |
| $a = 0.5$ | 0.226% | 0.225% | 0.224% | 0.223% | 0.221% | 0.219% | 0.217% | 0.215% | 0.213% |
| $a = 0.6$ | 0.231% | 0.230% | 0.229% | 0.227% | 0.225% | 0.223% | 0.221% | 0.220% | 0.218% |
| $a = 0.7$ | 0.235% | 0.234% | 0.234% | 0.232% | 0.230% | 0.228% | 0.226% | 0.225% | 0.223% |
| $a = 0.8$ | 0.240% | 0.239% | 0.239% | 0.237% | 0.235% | 0.233% | 0.231% | 0.230% | 0.229% |
| $a = 0.9$ | 0.245% | 0.244% | 0.244% | 0.242% | 0.240% | 0.238% | 0.236% | 0.235% | 0.234% |
| $a = 1$ | 0.250% | 0.249% | 0.248% | 0.248% | 0.246% | 0.243% | 0.242% | 0.240% | 0.240% |

The standard deviation of absolute value of SOC error under different parameter values is shown in Table 3.

**Table 3.** Standard deviation of the absolute value of SOC error under different parameter.

| | $M = 2$ | $M = 22$ | $M = 42$ | $M = 62$ | $M = 82$ | $M = 102$ | $M = 122$ | $M = 142$ | $M = 162$ |
|---|---|---|---|---|---|---|---|---|---|
| $a = 0$ | 0.735% | 0.735% | 0.735% | 0.735% | 0.735% | 0.735% | 0.735% | 0.735% | 0.735% |
| $a = 0.1$ | 0.716% | 0.716% | 0.715% | 0.714% | 0.712% | 0.711% | 0.710% | 0.710% | 0.710% |
| $a = 0.2$ | 0.700% | 0.700% | 0.699% | 0.696% | 0.693% | 0.691% | 0.690% | 0.690% | 0.690% |
| $a = 0.3$ | 0.686% | 0.687% | 0.685% | 0.682% | 0.678% | 0.675% | 0.674% | 0.674% | 0.674% |
| $a = 0.4$ | 0.674% | 0.676% | 0.675% | 0.671% | 0.665% | 0.662% | 0.660% | 0.660% | 0.661% |
| $a = 0.5$ | 0.664% | 0.667% | 0.666% | 0.662% | 0.655% | 0.651% | 0.649% | 0.650% | 0.651% |
| $a = 0.6$ | 0.655% | 0.659% | 0.659% | 0.655% | 0.647% | 0.642% | 0.640% | 0.641% | 0.642% |
| $a = 0.7$ | 0.648% | 0.653% | 0.653% | 0.649% | 0.641% | 0.634% | 0.632% | 0.633% | 0.635% |
| $a = 0.8$ | 0.641% | 0.647% | 0.649% | 0.645% | 0.635% | 0.628% | 0.625% | 0.626% | 0.629% |
| $a = 0.9$ | 0.636% | 0.643% | 0.645% | 0.642% | 0.631% | 0.623% | 0.620% | 0.621% | 0.624% |
| $a = 1$ | 0.631% | 0.639% | 0.642% | 0.640% | 0.629% | 0.619% | 0.615% | 0.616% | 0.619% |

It can be seen from Tables 2 and 3 that MIUKF + VFFRLS has advantages over the UKF + VFFRLS algorithm in a wide range of parameters. Nevertheless, it is still necessary to consider setting reasonable parameters to make the algorithm reach the state-of-the-art.

It also can be seen from Figure 5, Tables 2 and 3 that, as the value of $a$ increases, the standard deviation of the absolute value of SOC error decreases, but the average value of the absolute value of SOC error fluctuates from large to small and then to large. The fluctuation from large to small in the first part is characterized by the curve becoming more smooth in the figure, while the fluctuation from small to large in the second partis characterized by the curve becoming less smooth in the figure. Comparing the three-dimensional diagrams with different pitch angles when $M = 162$, as shown in Figure 6, it can be seen that the curve is less smooth when $a = 1$ than when $a = 0$, and there is obvious jitter at the time point close to convergence.

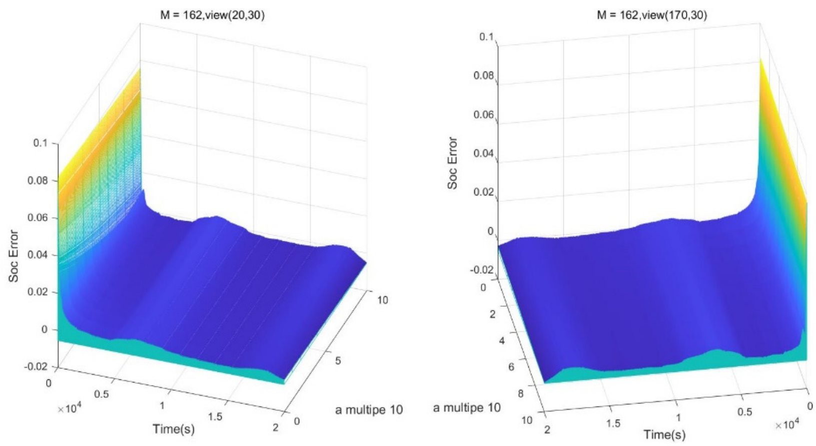


**Figure 6.** Three-dimensional SOC error diagrams with different pitch angles when $M = 162$.

The selection of MI model parameters is needed to improve the accuracy and stability of the algorithm as much as possible in order to reduce the mean and standard deviation of the estimated absolute error value. At the same time, it also needs to consider reducing the consumption of algorithm resources in order to reduce the value of $M$, which represents the time sliding window length. Considering the data comprehensively, $a = 0.5$ and $M = 22$ are selected in this paper.

### 5.3.2. Experiment Results of VFFRLS + MIUKF

(1) Current condition

The dynamic characteristics of the UUDS cycle are very strong, and the current changes almost every second. In the experimental process, the discharge is set at a positive number, the maximum discharge current is 62 A, and the maximum charging current is 41 A. The curve of the current over time is shown in Figure 7.

(2) Comparison between measured and estimated terminal voltage

The estimated terminal voltage of battery parameters is close to the measured terminal voltage, and the gap at the end of battery discharge is slightly enlarged, which is also consistent with the intuitive feeling that the internal polarization reaction of the battery tends to be intense at the end of battery discharge, resulting in the enhancement of nonlinear characteristics. The maximum error of terminal voltage is 20.3%, the minimum value is −7.87%, and the average value of the absolute error is 0.57%. The time-varying terminal voltage curve of the measured value and estimated value and the time-varying curve of the terminal voltage error are shown in Figures 8 and 9, respectively.

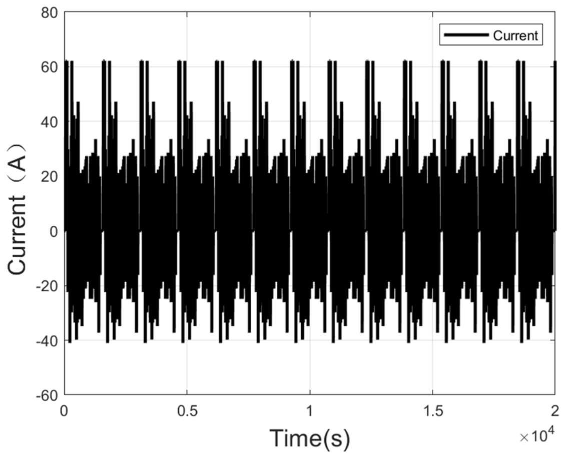


**Figure 7.** Discharge current over time.

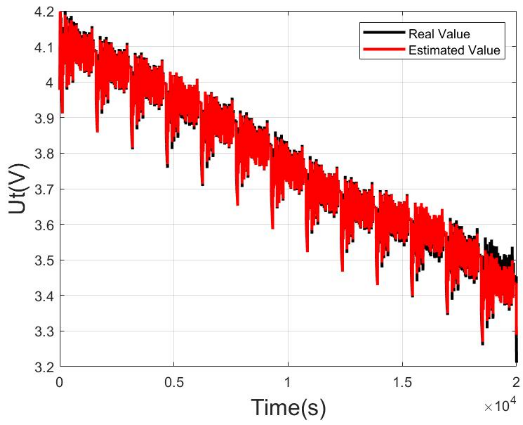


**Figure 8.** Curve of measured and estimated terminal voltage values over time.

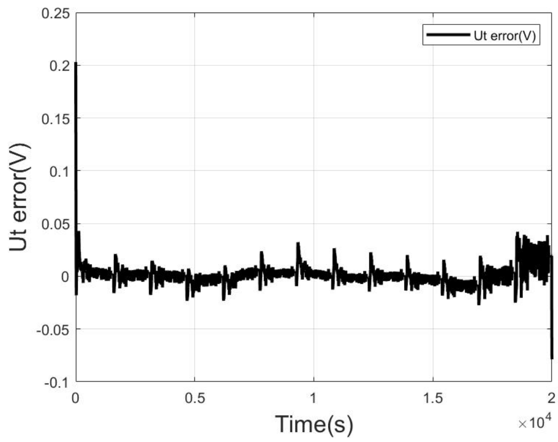


**Figure 9.** Curve of terminal voltage error over time.

(3) Identification results of battery resistance and capacitance parameters

The parameters related to the resistance and capacitance of the battery identified by the algorithm are shown in the Figure 10.

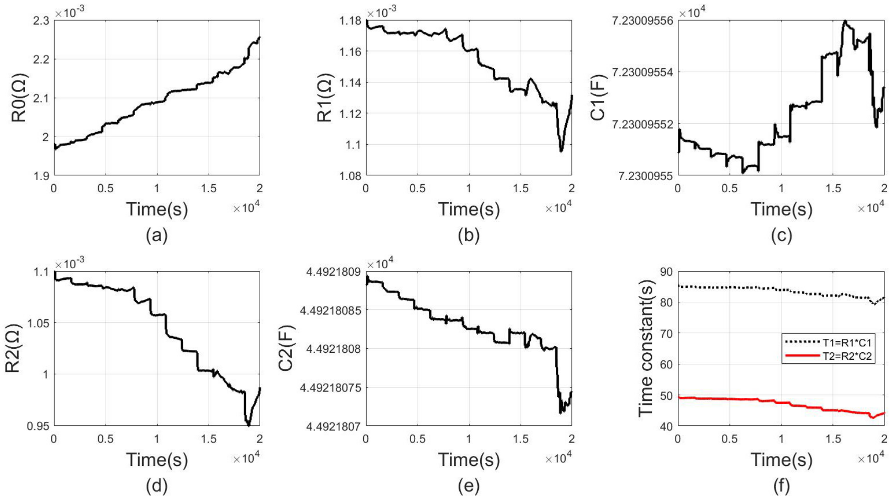


**Figure 10.** Identification results of battery resistance and capacitance parameters.: (**a**) R0 result, (**b**) R1 result, (**c**) C1 result, (**d**) R2 result, (**e**) C2 result, (**f**) T1 and T2 results.

R0 represents ohmic internal resistance, and its size depends on the activation degree of the electrode and active material which decreases with the decrease in SOC. Therefore, generally speaking, R0 shows a gradual increase trend with the passage of discharge time—that is, it gradually increases with the decrease in SOC. The identified R0 parameters conform to this physical characteristic.

R1 and C1 are represented as slow reaction polarization phenomena in the model, and R2 and C2 are represented as fast reaction polarization phenomena in the model. Their respective products are called time constants, which should conform to R1 * C1 > R2 * C2, and the identified parameters also conform to this physical feature.

It is worth noting that, similarly to R0, R1 and R2 generally increase gradually with the decrease in SOC. The parameters identified in this paper are inconsistent with this. Considering that this goal is not present in the model, and the inconsistency here does not cause significant deviation from the preset objectives of the model, the identification results are still successful.

(4) SOC estimate vs. baseline

The maximum value of SOC error is 19%, the minimum value is −0.44%, and the average value of absolute value is 0.225%. The SOC estimation value of the algorithm can quickly adjust the gap with the reference value. After 114 sampling cycles—that is, 114 s—the error of the algorithm decreases from 19% to less than 5%, and after 416 s, it decreases to less than 1%, after which it remains below 1%.

The time-varying curves of SOC estimated value and reference value and the time-varying curves of error are shown in Figures 11 and 12, respectively.

### 5.3.3. Comparison of Algorithm Experiment Results

Based on the same data, the online parameter estimation algorithm VFFRLS + UKF and the offline parameter estimation algorithm MIUKF, the UKF and EKF, are used for the experiment. The comparison between the online and offline algorithms is based on similar cost baselines, as it is difficult to compare them in other aspects, so the same offline resistance and capacitance parameters are used as initial value for online parameters, and the same system and measurement noise covariance matrix are used as well. The comparison results show that the online parameter estimation has obvious advantages in accuracy and stability—the average value of the absolute value of the error is small, and the error curve is stable and close to zero over time. Compared with the VFFRLS + UKF algorithm of the estimation of the same online parameter, VFFRLS + MIUKF is superior in convergence speed, accuracy and stability, which shows that the error converges to zero faster, and the average absolute value of the error and the standard deviation of the error are small.

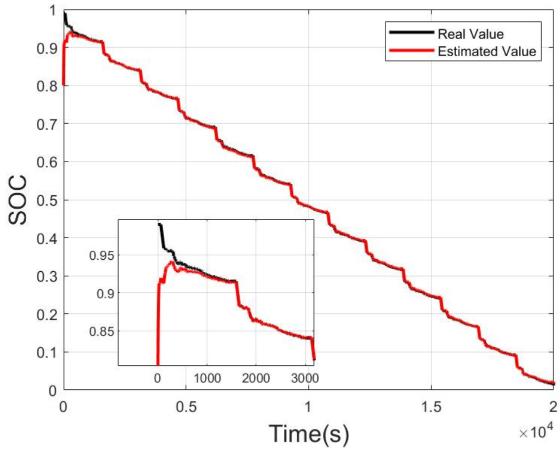


**Figure 11.** Curve of SOC estimated value and reference value over time.

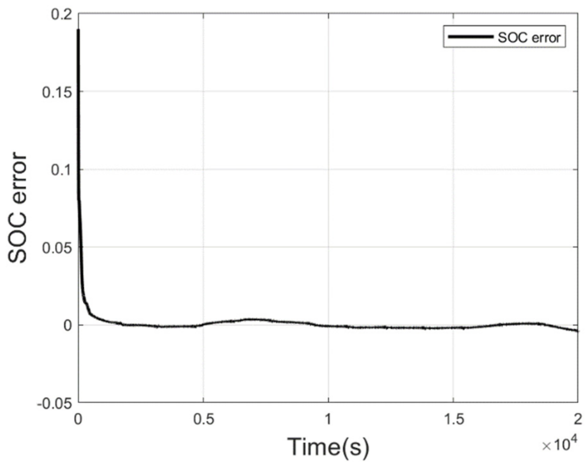


**Figure 12.** Curve of SOC estimation error over time.

The index statistics related to the stability, accuracy and convergence speed of the SOC prediction error results of each algorithm are shown in Table 4.

**Table 4.** The index statistics related to the stability, accuracy and convergence speed of the SOC prediction error results of each algorithm.

| Algorithm | Maximum Error Value | Minimum Error Value | Average Absolute Values of Error | Standard Deviation of Error Value | The First Time When the Absolute Value of the Error Starts to Be Less than the Average Value | The Second Time When the Absolute Value of the Error Begins to Be Greater than the Average Value |
|---|---|---|---|---|---|---|
| VFFRLS + MIUKF | 19.00% | −0.44% | 0.23% | 0.67% | 1138 s | 6012 s |
| VFFRLS + UKF | 19.00% | −0.34% | 0.25% | 0.74% | 1835 s | 6014 s |
| MIUKF | 19.00% | −1.14% | 0.78% | 1.22% | 408 s | 3331 s |
| UKF | 19.00% | −1.92% | 1.02% | 0.88% | 25 s | 3310 s |
| EKF | 19.00% | −2.65% | 1.20% | 0.49% | 7 s | 158 s |

The curve of the SOC predicted value and reference value of each algorithm over time is shown in Figure 13.

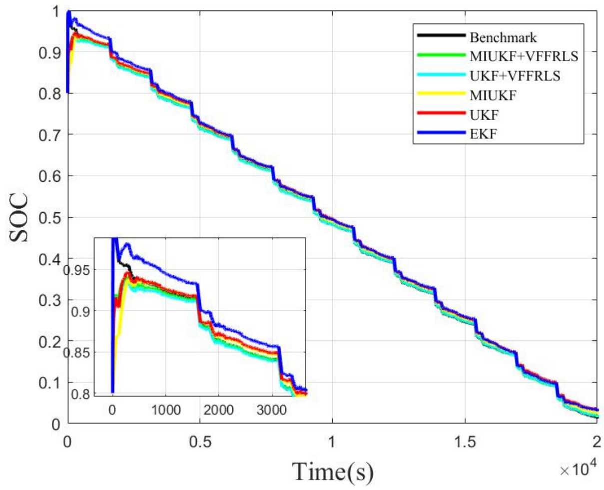


**Figure 13.** The curve of the SOC predicted value and reference value of each algorithm over time.

The time-varying curve of the SOC prediction error of each algorithm is shown in Figure 14.

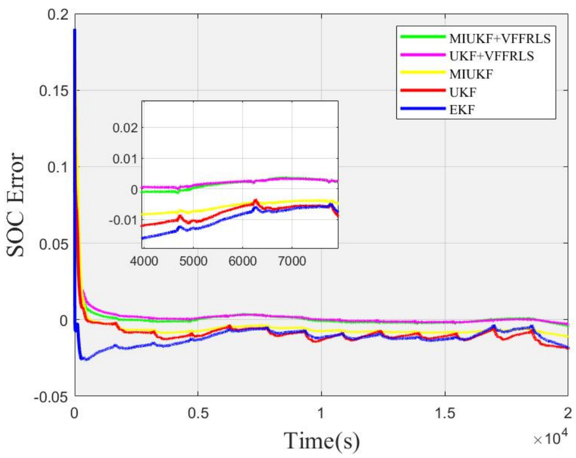


**Figure 14.** The time-varying curve of SOC prediction error of each algorithm.

## 6. Conclusions

Accurate and real-time SOC estimation is the basis and key to realizing balanced battery management, which can reduce battery internal resistance loss and the possibility of battery overcharge and discharge. Due to the complex internal chemical and physical reactions and dynamic environmental conditions, the SOC of a battery has obvious nonlinear and time-varying characteristics, which has always been the focus of and main difficulty in battery management system research.

In this paper, a joint SOC estimation algorithm based on online parameter identification and a second-order RC equivalent circuit model is proposed, which innovatively realizes the dual estimation of MIUKF + VFFRLS. The experimental results based on UDDS test data show that the algorithm has obvious advantages in stability and accuracy compared with offline parameter + EKF, offline parameter + UKF and offline parameter +MIUKF; compared with UKF + VFFRLS, it has advantages in convergence speed, accuracy and stability. The overall performance of the fused algorithm is outstanding.

Through the above research work, the SOC estimation accuracy can be effectively improved, the battery consistency management ability can be improved, and the theoretical value and practical value can be reflected, but there are still limitations and deficiencies.

The tuning of the KF is critical to the SOC estimation results, and optimization methods can be further discussed. The accuracy of RLS algorithm is very sensitive to measurement noise, and the associated noise-compensation methods can be further studied. The model-based SOC estimation also depends on accurate estimation of the battery capacity, and data-based capacity estimation can be further studied.

The applicability of the algorithm is also related to the efficiency of the algorithm. The calculation time of the algorithm is not compared in this experiment because the calculation time is strongly related to factors such as the type of program language and the method of coding. The battery type used in the algorithm is a ternary lithium battery with a relatively strong linear relationship between the $U_{ocv}$ and the SOC curve. The duration of experimental data is short. The factors of battery capacity attenuation and temperature change are not considered.

The follow-up research can work in the following directions: making noise-compensated methods research [22,23], optimizing the tuning of the KF [24], considering the factors of battery capacity attenuation [25] and temperature change, designing an analogous algorithm efficiency model to compare the calculation time of different types of SOC estimation algorithms, performing experiments to collect data for a longer time or to seek a larger public dataset, further verifying the effectiveness of the algorithm based on larger datasets with different batteries, further studying the effectiveness of intelligent algorithms such as neural networks and the algorithm proposed by this paper in large data sets and exploring more efficient SOC estimation methods suitable for more scenarios.

**Author Contributions:** Conceptualization, H.Y. and H.P.; methodology, H.Y. and Y.H.; software, H.Y.; validation, H.Y., Y.H. and Y.Z.; formal analysis, J.D.; investigation, H.Y. and Y.H.; resources, Y.Z.; data curation, Z.C.; writing—original draft preparation, H.Y.; writing—review and editing, Y.H.; visualization, H.Y.; supervision, H.P.; project administration, H.P.; funding acquisition, J.D. All authors have read and agreed to the published version of the manuscript. H.Y. and Y.H. contributed equally to this work.

**Funding:** This research was funded by the project 2021 Natural Science Foundation of Guangdong Province, Grant No. is 2021A1515011851.

**Conflicts of Interest:** The authors declare no conflict of interest.

## References


1. Rivera-Barrera, J.P.; Muñoz-Galeano, N.; Sarmiento-Maldonado, H.O. SoC estimation for lithium-ion batteries: Review and future challenges. *Electronics* **2017**, *6*, 102. [CrossRef]
2. Hong, J.; Wang, Z.; Chen, W.; Wang, L.-Y.; Qu, C. Online joint-prediction of multi-forward-step battery SOC using LSTM neural networks and multiple linear regression for real-world electric vehicles. *J. Energy Storage* **2020**, *30*, 101459. [CrossRef]
3. Zhao, F.; Li, Y.; Wang, X.; Bai, L.; Liu, T. Lithium-ion batteries State of Charge prediction of electric vehicles using RNNs-CNNs neural networks. *IEEE Access* **2020**, *8*, 98168–98180. [CrossRef]
4. Liu, X.; Li, K.; Wu, J.; He, Y.; Liu, X. An extended Kalman filter based data-driven method for State of Charge estimation of Li-ion batteries. *J. Energy Storage* **2021**, *40*, 102655. [CrossRef]
5. Al-Gabalawy, M.; Hosny, N.S.; Dawson, J.A.; Omar, A.I. State of Charge estimation of a Li-ion battery based on extended Kalman filtering and sensor bias. *Int. J. Energy Res.* **2021**, *45*, 6708–6726. [CrossRef]
6. Zhao, Y.; Xu, J.; Wang, X.; Mei, X. The Adaptive Fading Extended Kalman Filter SOC Estimation Method for Lithium-ion Batteries. *Energy Procedia* **2018**, *145*, 357–362. [CrossRef]
7. Wang, W.; Wang, X.; Xiang, C.; Wei, C.; Zhao, Y. Unscented kalman filter-based battery SOC estimation and peak power prediction method for power distribution of hybrid electric vehicles. *IEEE Access* **2018**, *6*, 35957–35965. [CrossRef]
8. Xing, J.; Wu, P. State of Charge estimation of lithium-ion battery based on improved adaptive unscented kalman filter. *Sustainability* **2021**, *13*, 5046. [CrossRef]
9. Peng, X.; Li, Y.; Yang, W.; Garg, A. Real-Time State of Charge Estimation of the Extended Kalman Filter and Unscented Kalman Filter Algorithms Under Different Working Conditions. *J. Electrochem. Energy Convers. Storage* **2021**, *18*, 041007. [CrossRef]
10. Li, W.; Yang, Y.; Wang, D.; Yin, S. The multi-innovation extended Kalman filter algorithm for battery SOC estimation. *Ionics* **2020**, *26*, 6145–6156. [CrossRef]

11. Zahid, T.; Li, W. A Comparative Study Based on the Least Square Parameter Identification Method for State of Charge Estimation of a LiFePO4 Battery Pack Using Three Model-Based Algorithms for Electric Vehicles. *Energies* **2016**, *9*, 720. [CrossRef]
12. Lin, C.; Zhang, X.H. Modeling and Simulation Research on Lithium-Ion Battery in Electric Vehicles Based on Genetic Algorithm. *Appl. Mech. Mater.* **2014**, *494–495*, 246–249. [CrossRef]
13. He, H.; Zhang, X.; Xiong, R.; Xu, Y.; Guo, H. Online model-based estimation of state-of-charge and open-circuit voltage of lithium-ion batteries in electric vehicles. *Energy* **2012**, *39*, 310–318. [CrossRef]
14. He, H.; Xiong, R.; Guo, H. Online estimation of model parameters and state-of-charge of $LiFePO_4$ batteries in electric vehicles. *Appl. Energy* **2012**, *89*, 413–420. [CrossRef]
15. Tong, S.; Klein, M.P.; Park, J.W. On-line optimization of battery open circuit voltage for improved state-of-charge and state-of-health estimation. *J. Power Sources* **2015**, *293*, 416–428. [CrossRef]
16. Ouyang, T.; Xu, P.; Chen, J.; Lu, J.; Chen, N. Improved parameters identification and State of Charge estimation for lithium-ion battery with real-time optimal forgetting factor. *Electrochim. Acta* **2020**, *353*, 136576. [CrossRef]
17. Xiong, R.; Sun, F.; Chen, Z.; He, H. A data-driven multi-scale extended Kalman filtering based parameter and state estimation approach of lithium-ion polymer battery in electric vehicles. *Appl. Energy* **2014**, *113*, 463–476. [CrossRef]
18. Lao, Z.; Xia, B.; Wang, W.; Sun, W.; Lai, Y.; Wang, M. A novel method for lithium-ion battery online parameter identification based on variable forgetting factor recursive least squares. *Energies* **2018**, *11*, 1358. [CrossRef]
19. Waag, W.; Fleischer, C.; Sauer, D.U. On-line estimation of lithium-ion battery impedance parameters using a novel varied-parameters approach. *J. Power Sources* **2013**, *237*, 260–269. [CrossRef]
20. He, H.; Xiong, R.; Fan, J. Evaluation of Lithium-Ion Battery Equivalent Circuit Models for State of Charge Estimation by an Experimental Approach. *Energies* **2011**, *4*, 582–598. [CrossRef]
21. US EPA. Urban Dynamometer Driving Schedule, Emission Standards Reference Guide [EB/OL]. USA. 2017. Available online: https://www.epa.gov/vehicle-and-fuel-emissions-testing/dynamometer-drive-schedules (accessed on 25 November 2021).
22. Wei, Z.; Zou, C.; Leng, F.; Soong, B.H.; Tseng, K.-J. Online model identification and state-of-charge estimate for lithium-ion battery with a recursive total least squares-based observer. *IEEE Trans. Ind. Electron.* **2018**, *65*, 1336–1346. [CrossRef]
23. Wei, Z.; Zhao, J.; Xiong, R.; Dong, G.; Pou, J.; Tseng, K.J. Online estimation of power capacity with noise effect attenuation for lithium-ion battery. *IEEE Trans. Ind. Electron.* **2019**, *66*, 5724–5735. [CrossRef]
24. He, J.; Wei, Z.; Bian, X.; Yan, F. State-of-Health Estimation of Lithium-Ion Batteries Using Incremental Capacity Analysis Based on Voltage–Capacity Model. *IEEE Trans. Transp. Electrif.* **2020**, *6*, 417–426. [CrossRef]
25. Bian, X.; Wei, Z.; He, J.; Yan, F.; Liu, L. A Two-Step Parameter Optimization Method for Low-Order Model-Based State-of-Charge Estimation. *IEEE Trans. Transp. Electrif.* **2021**, *7*, 399–409. [CrossRef]